Flow visualisation of the helicopter brown-out phenomenon

N. D. Nathan

Department of Aerospace Engineering
University of Glasgow
Glasgow, Scotland
UK

R. B. Green
richardg@aero.gla.ac.uk

ABSTRACT

Quantitative and qualitative results of a series of experiments conducted on a rotor in ground effect at low forward speeds are presented. The velocity over a wide area of the ground effect wake was measured using particle image velocimetry, and the evolution of the flow is described as the forward speed increases. The formation of a dust cloud leading to so-called helicopter brown-out was simulated through a series of flow visualisation experiments. The technique involved sprinkling a fine dust on the ground below and ahead of the rotor. Larger dust clouds were observed at lower forward speed, and the dust cloud penetrated into the areas of the flow including those where vorticity levels were of low magnitude and occasional velocity fluctuations from the mean were large.

NOMENCLATURE

c	blade chord, (m)
h	rotor height above the ground, m
r	radial co-ordinate along rotor disk, m
u	horizontal velocity component, ms^{-1}
v	vertical velocity component, ms^{-1}
y	vertical co-ordinate, m
A	rotor disk area, m^2
C_T	hover thrust coefficient, $\frac{T}{\rho A V_{tip}^2}$
D	rotor diameter, (m)
R	rotor radius, (m)
T	rotor thrust, (N)
U_∞	flight speed, wind-tunnel speed, ms^{-1}
V_h	hover induced velocity $V_{tip}\sqrt{\frac{C_T}{2}}$, ms^{-1}
V_{tip}	rotor blade tip velocity, ms^{-1}
μ	advance ratio, $\frac{U_\infty}{V_{tip}}$
μ^*	normalised advance ratio, $\frac{\mu}{\sqrt{C_T/2}}$
ν	fluid kinematic viscosity, m^2s^{-1}
ρ	fluid density, kgm^{-3}
ω	vorticity $\frac{\partial v}{\partial r}-\frac{\partial u}{\partial y}$, $rads^{-1}$
Γ	rotor blade tip vortex circulation, m^2s^{-1}
GE	ground effect
IGE	in ground effect
OGE	out of ground effect
PIV	particle image velocimetry

1.0 INTRODUCTION

When a helicopter is operating close to the vicinity of the ground, the rotor is said to be in ground effect. The fluid dynamics of the rotor wake IGE are significantly different to that of a rotor operating out of ground effect. There are various performance advantages and benefits IGE, but ground effect also leads to some operational difficulties. For example, when a helicopter is close to a dusty or sandy ground, the downwash from the rotor system can lift loose matter off the ground to create a cloud that can envelop the entire aircraft. The

Paper No. 3379. Manuscript received 28 November 2008, revised version received 6 April 2009 accepted 30 April 2009.

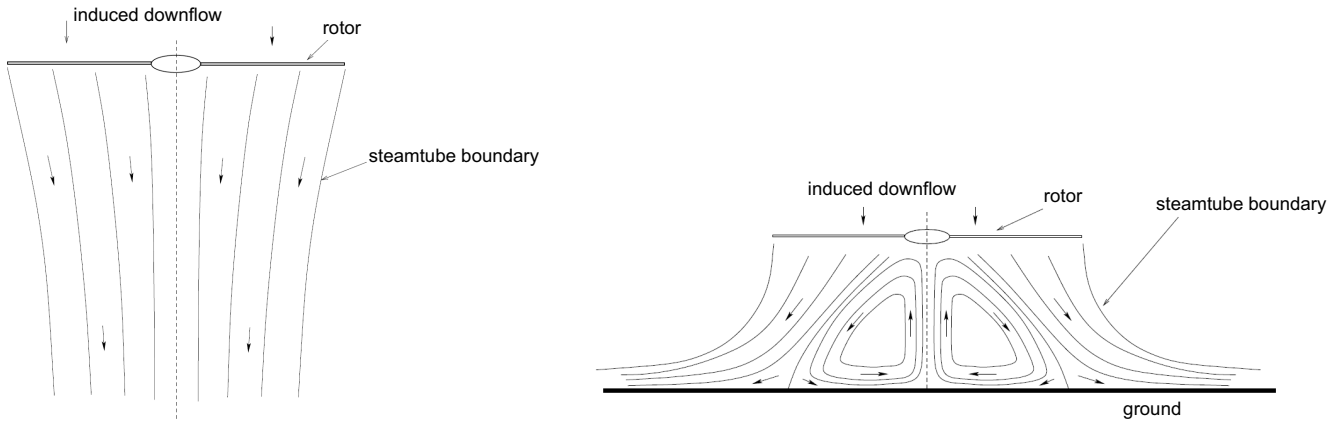

(a) Hover OGE (b) Hover IGE

Figure 1. Comparison between OGE and IGE wake of a hovering rotor. The figure shows schematic diagrams of mean flow streamlines.

consequence of this is that the pilot may lose all visual cues and become disoriented, which may lead to so-called brown-out; American defence sources suggest over 200 cases of aircraft damage or injury to personnel since 1991 due to this phenomenon.

Performance related experiments on rotor IGE flow have commanded the most interest as it has been observed that the power required to hover IGE is significantly lower than OGE[1,2,3,4]. This power reduction, observed experimentally on numerous occasions[3,5,6], has been confirmed to exist up to a ground height (i.e. h/D) of around one, after which the ground is not seen to have any significant effect on the rotor performance. This has in turn encouraged research interests in both mathematical and computational modelling of rotor performance IGE[6,7,4]. The most obvious difference in the wake of a hovering rotor IGE is the expansion of the wake instead of the classical contraction seen OGE[4], illustrated in Fig. 1. In the case of the hovering rotor in ground effect, the tip vortices pass very close to the ground, and the formation of the dust cloud in hover at least is due to the manner in which the tip vortices pass over the ground and pick up loose material, and then how this material is advected.

In the forward flight case the majority of rotor IGE experimental research has concentrated on low advance ratio μ. The advance ratio is a non-dimensional forward speed, but in many respects the normalised advance ratio μ^* is better used as it accounts for the thrust induced downward flow below the rotor. While most ground effect research has been conducted in order to analyse the performance implications of the ground on a rotor operating at low advance ratio[4], limited quantitative analysis has been performed to determine the wake characteristics. In ground effect in forward flight, a range of flow regimes have been observed; at very low advance ratio a recirculation loop is observed whilst at higher advance ratio a compact ground vortex forms[8] (see Fig. 2.). The flight regimes, broadly defined by Curtiss *et al*[3,5], are best expressed in terms of the normalised advance ratio given by $\mu*$. The recirculation regime is observed to occur in the range $0{\cdot}4 < \mu* < 0{\cdot}7$, where the rotor blade tip vortices recirculate in a loop ahead of the rotor disk. This loop is formed as tip vortices pass along the ground ahead of the rotor and then move in an arc upwards and back towards the rotor disk, where reports suggest a re-ingestion of the wake vortices through the rotor disk[5,9,10], and the recirculation loop has been observed to increase the inflow through the forward portion of the rotor[11]. Examination of the mean flow shows a separation point at the most upstream extent of the recirculation zone, and as advance ratio increases the separation point moves towards the rotor. Using hot-wire anemometry, between $0{\cdot}04 < \mu < 0{\cdot}06$ with the rotor at $h/D = 0{\cdot}36$[10], Saijo *et al*, observed the separation point to oscillate back and forth with large amplitude, while in the range $0{\cdot}06 < \mu < 0{\cdot}1$ it appeared to be in a more stationary position. Successful computation of these low advance ratio forward flight regimes has been achieved by Brown and Whitehouse[7]. For higher advance ratio, $\mu^* > 0{\cdot}7$, a well-defined, concentrated ground vortex is seen to form[3]. Its formation is generally noted to be a function of μ^* and ground height[12]. Flow visualisations done by Sheridan and Wiesner, suggest that the ground vortex is formed as the spreading wake ahead of the rotor disk is decelerated and stopped by the free-stream, causing the flow along the ground to separate and roll up[8]. Increasing advance ratio results in the ground vortex gaining prominence, with part of the freestream being entrained into the ground vortex and part of it being ingested into the rotor. This additional inflow through the rotor is thought to increase the power required by the rotor, reducing the performance benefits experienced by the rotor in hover IGE[4]. The ground vortex is seen to move towards the rotor as advance ratio is further increased. When the ground vortex is just beneath the leading edge of the rotor, the inflow through the rotor induced by the ground vortex is at its maximum, as seen in Fig. 2(c). The power required during this stage is equal to, or just below the power required OGE, as identified during performance analysis. The ground vortex continues to move further downstream, away from the leading edge of the rotor disk, with increasing advance ratio. This movement reduces the inflow through the rotor disk, as can be seen from Fig. 2(d), and also results in some amount of upflow through the disk[8], reducing the power required compared to when the ground vortex was just below the leading edge of the rotor disk. As the ground vortex continues to move further downstream, it is seen to lose its strength and diminish in size, eventually disappearing from the wake as the advance ratio, reaches $\mu = 0{\cdot}12$[12] or around $\mu* = 1{\cdot}3$.

Flow visualisation experiments, conducted by Boyd *et al*[13], using smoke and tufts on the ground indicate the presence of an interaction boundary on the ground when in forward flight. The interaction boundary is formed as the wake from the rotor encounters the oncoming free-stream. The boundary is seen to move towards the rotor as the free-stream velocity increases. Furthermore the symmetry of the interaction boundary depends on the rotor used. If the rotor is rigid, the inability for the rotor to compensate for the differential lift produced in the advancing and retreating sides of the rotor results in the formation of an asymmetric interaction boundary on the ground. This boundary is otherwise symmetric and parabolic in shape, if the rotor is allowed to trim or during hover[14]. A particle image velocimetry (PIV) investigation of the ground vortex regime, conducted by Ganesh and Komerath, showed the influence of the tip vortex system on the formation of the ground vortex [15].

https://doi.org/10.1017/S0001924000003134 Published online by Cambridge University Press

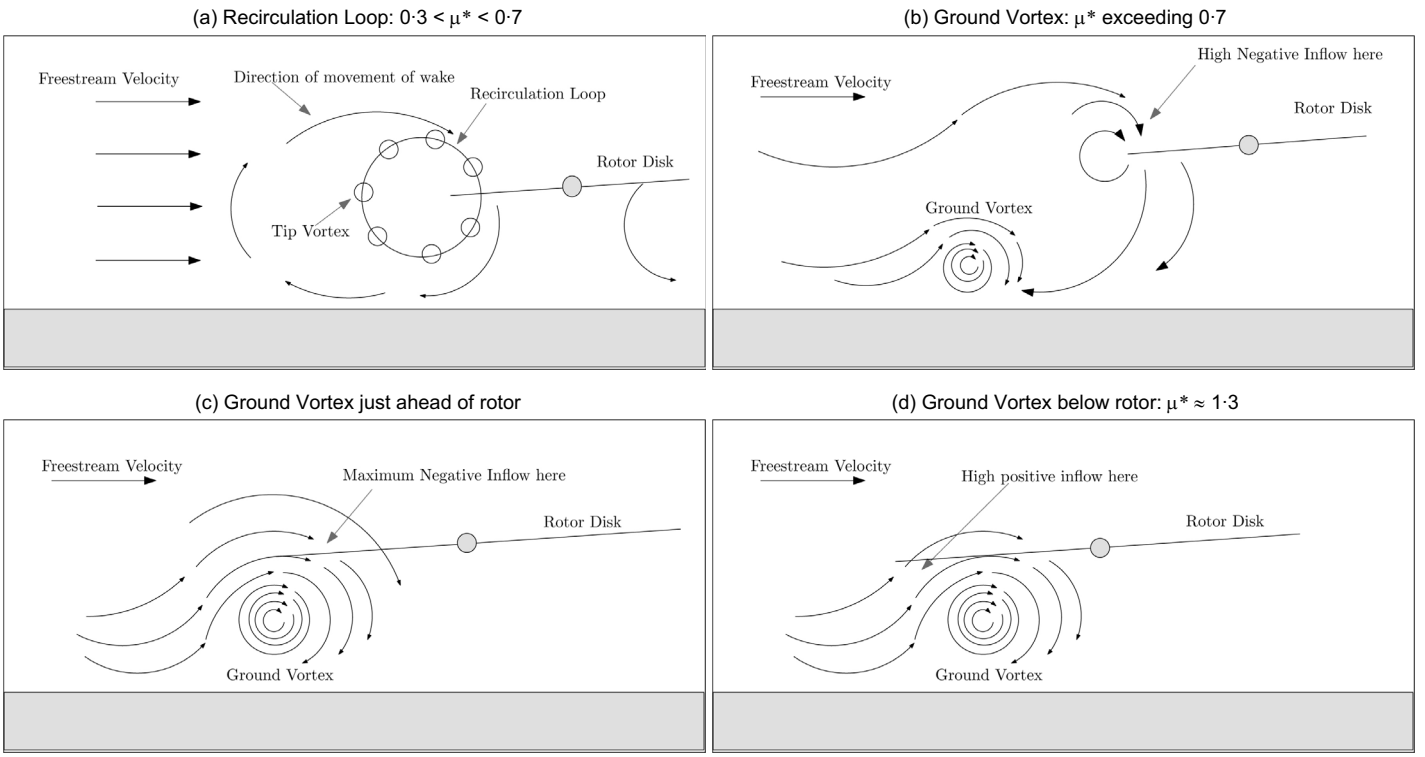

Figure 2. Schematic of the ground effect flow at varying advance ratios[8]. The recirculation regime is shown in frames (a) and (b) and the ground vortex regime in frames (c) and (d).

The forward flight IGE flow field is far more complicated than the hover IGE flow, but it immediately appears that the formation of a ground effect induced dust cloud that leads to pilot brown-out must again be due to the action on the ground of the vortex system trailed below the rotor and the subsequent behaviour of the material that is swept up forward of the rotor. Improved understanding of the flow field is a necessary pre-cursor to gaining knowledge of the brown-out dust cloud, but it is interesting to determine how the brown-out dust cloud correlates with the position of the tip vortices and their fragments. This paper presents results of an experimental study of ground effect in forward flight and an investigation of the formation of a dust cloud to simulate the conditions for brown-out. No attempt has been made to measure the loss of visual cues that the pilot might experience, and the emphasis of the investigation is on the fluid dynamics.

2.0 EXPERIMENTAL METHODS

The experiments were performed in two different wind tunnels using a simple rotor rig. Rotor wake phenomena were investigated using flow visualisation and PIV. The techniques are described below.

2.1 Rotor rig

Due to the limitations imposed by the physical dimensions of the wind-tunnel facilities available and the huge spatial extent of the ground effect wake, it was necessary to use a small-scale rotor system for these investigations. This means that the chord Reynolds number will be particularly low (around 40,000). The main issue of concern regarding the fluid dynamics is the circulation Reynolds number Γ/ν. If this is above a moderate value at least 10,000 or so, then the vortex wake dynamics will be inertia dominated[16] and may be regarded as representative of those of a much larger scale system.

The rotor rig that was used for these investigations was based on readily available propellers designed for model aircraft. These propellers produce a useful vortex wake that is representative of a helicopter rotor wake in that it consists of inter-twined, helical vortices, and hence were deemed suitable for use in an experimental rotor rig. For the purposes of these experiments, a two-bladed model aircraft propeller manufactured by Graupner was used. The propeller diameter, maximum chord (at 50% span) and tip chord were 15cm, 1·05cm and 0·8cm respectively. No feather or collective angle was available, but the propeller pitch was 7·5cm with about 10° of twist. It is not clear what aerofoil section(s) are used for these propellers, although they are cambered, and the maximum thickness was 16·4% at the 50% span position. The propellers were fixed onto the shaft of a small d.c. electric motor capable of spinning the rotor at a rate of 7,200rpm. The rotor speed was monitored using a stroboscope, and the thrust was measured by mounting the motor on a 0·6kg load-cell. This assembly was fixed to the end of a long sting attached to a hand-cranked vertical traverse unit, which was placed on the ground so that the rotor disk was nominally in the horizontal plane with the motor above the disk. The rotor support mechanism was not observed to have any measurable effect on the in-flow to the rotor or to the flow field around the rotor. A schematic diagram of the apparatus is shown in Fig. 3.

2.2 Wind-tunnel facilities

Quantitative investigations of the ground effect wake using PIV were conducted in a 1·05m × 0·85m working section, closed return wind tunnel with a contraction ratio of 9:1, capable of a top speed of some 30ms^{-1}. A raised ground board spanning the tunnel width had to be placed into the working section due to limited optical access, and the rotor was placed on this ground board; the ratio of rotor diameter to ground board width was 0·143. Flow visualisation of the dust cloud was conducted in a different facility. This wind tunnel has a 0·91m × 0·91m square, 4m long working section, and is a closed, non-return type, with a settling chamber and 9:1 contraction at the upstream end and a fan at the downstream end. The maximum speed of this tunnel is some 2·5ms^{-1}, and the rotor assembly is simply placed on the floor of the tunnel.

https://doi.org/10.1017/S0001924000003134 Published online by Cambridge University Press

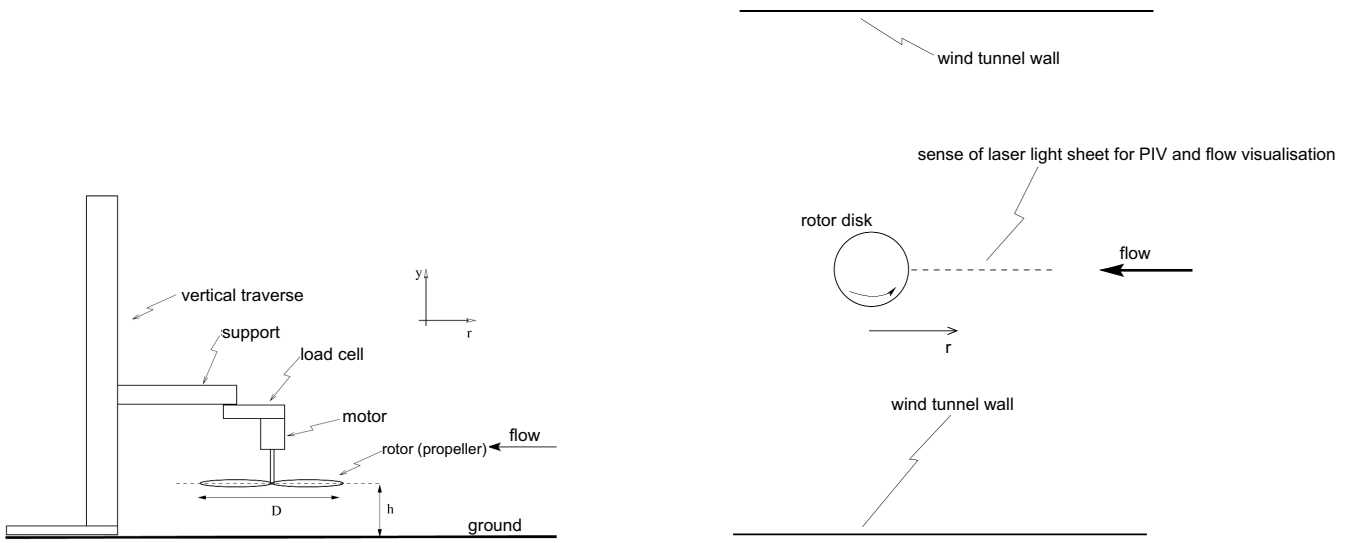

(a) Rotor system

(b) Plan view showing laser sheet position

Figure 3. Schematic diagram of rotor system, motor, load-cell and vertical traverse. The sense of the (*r,y*) coordinate system is shown, but its origin is at the centre of the rotor; the direction *r* is directly ahead of the rotor, *y* is vertically upwards, and the (*r,y*) plane is aligned with the longitudinal axis of the wind tunnel. Frame (a) shows the rotor above the ground, and frame (b) shows a plan view of the system and the relative position of the laser light sheet for flow visualisation.

2.3 PIV facility

Quantitative analysis of the wake of the rotor IGE forward flight was performed using two-component PIV, which allows for the measurement of the (*u,v*) velocity components of the flow field. Double frame, double exposure PIV was used, for which two seeded flow images, separated by a known time delay Δt, are recorded and used to infer the (*u,v*) velocity field. The region of interest was in the (*r,y*) plane of the rotor (see Fig 3) ahead of the rotor axis, and illuminated by a 2mm thick laser light sheet produced by a Spectra-Physics Lab130-10 Nd:YAG single cavity, double pulsed, frequency doubled laser, with a wavelength of 532nm and a pulse duration of 8ns. A Kodak MegaPlus ES1.0 digital video camera, with a 1,018 × 1,008 pixel CCD chip, fitted with a 50mm focal length Nikkor lens set to *f*/2·4, was used for image recording. Seeding was produced using a Concept Systems ViCount smoke generator that heats smoke oil to produce a fine oil mist; the manufacturer claims a nominal seeding particle diameter of 0·2μm. Image capture was done using a National Instruments PCI-1424 digital frame grabber operated using LABVIEW. The laser, camera control and image capture systems were all synchronised using a National Instruments PCI-TI0-10 counter timer card and controlled by a single computer. In cases where a wider field of view was required, a higher resolution Redlake MegaPlus 4 digital video camera with a 2,048 × 2,048 pixel CCD chip was used. This camera was used especially with the lower advance ratio cases, where the wake was seen to spread beyond one diameter from the rotor disk leading edge. The PIV system image capture and rotor azimuth were unrelated in phase.

Analysis of the images by successive cross-correlation and Lagrangian tile-shifting produces high-resolution velocity vector maps. The procedure starts with a low-resolution pass, and the results of this drive the high-resolution analysis. For each IGE test, 300 image pairs with a set PIV time delay of Δt = 90μm were taken; thus 300 vector fields for each case were recorded, which is sufficient for meaningful average and root-mean-square velocity statistics to be derived. The spatial resolution of the measurements is clearly dictated by the field of view, but for the current experiments, where the field of view was around one rotor diameter square, the effective measurement area per point was around 0·016*D* × 0·016*D*. The velocity estimation accuracy is better than 2%, but data loss is severe in the region of the tip vortices due to their small size relative to the large field of view. Tip vortex cores immediately below the rotor disk were around 0·06*D* in diameter, meaning that only four or so velocity points were evaluated across the diameter of the tip vortex vorticity core (hence around 16 velocity points in total inside the tip vortex core). PIV tends to produce results biased to the lower velocity in regions of high velocity gradient flow sampled at low spatial resolution. Thus the velocity accuracy inside the vortex cores will inferior to elsewhere, and when combined with the small number of measurement points across the vortex core this means the peak vorticity magnitudes are underestimated. The drawbacks of the use of PIV to measure vortex cores are well known, and great care is required in its use to evaluate the vortex core properties with accuracy[17]. However the aim of the experiment was to visualise the larger area of the rotor wake and not concentrate on the precise details of the vortex cores. Note that the circulation of a tip vortex can be calculated with a great degree of confidence if the calculation is based around a large contour outside the area of large velocity gradient.

2.4 Simulation of the helicopter brown-out

The development of the dust cloud that leads to helicopter brown-out was studied by flow visualisation in a wind tunnel. For the purposes of these tests, talcum powder was used as the material to simulate the brown-out dust cloud. The talcum powder was introduced into the flow by spreading it in a thin layer along the floor of the wind tunnel ahead of the rotor. At the rotor speed and wind-tunnel speed setting used it was observed that the talcum powder was lifted off the ground by the action of the rotor induced flow alone. Due to the depletion of the talcum powder layer during the experiment and

https://doi.org/10.1017/S0001924000003134 Published online by Cambridge University Press

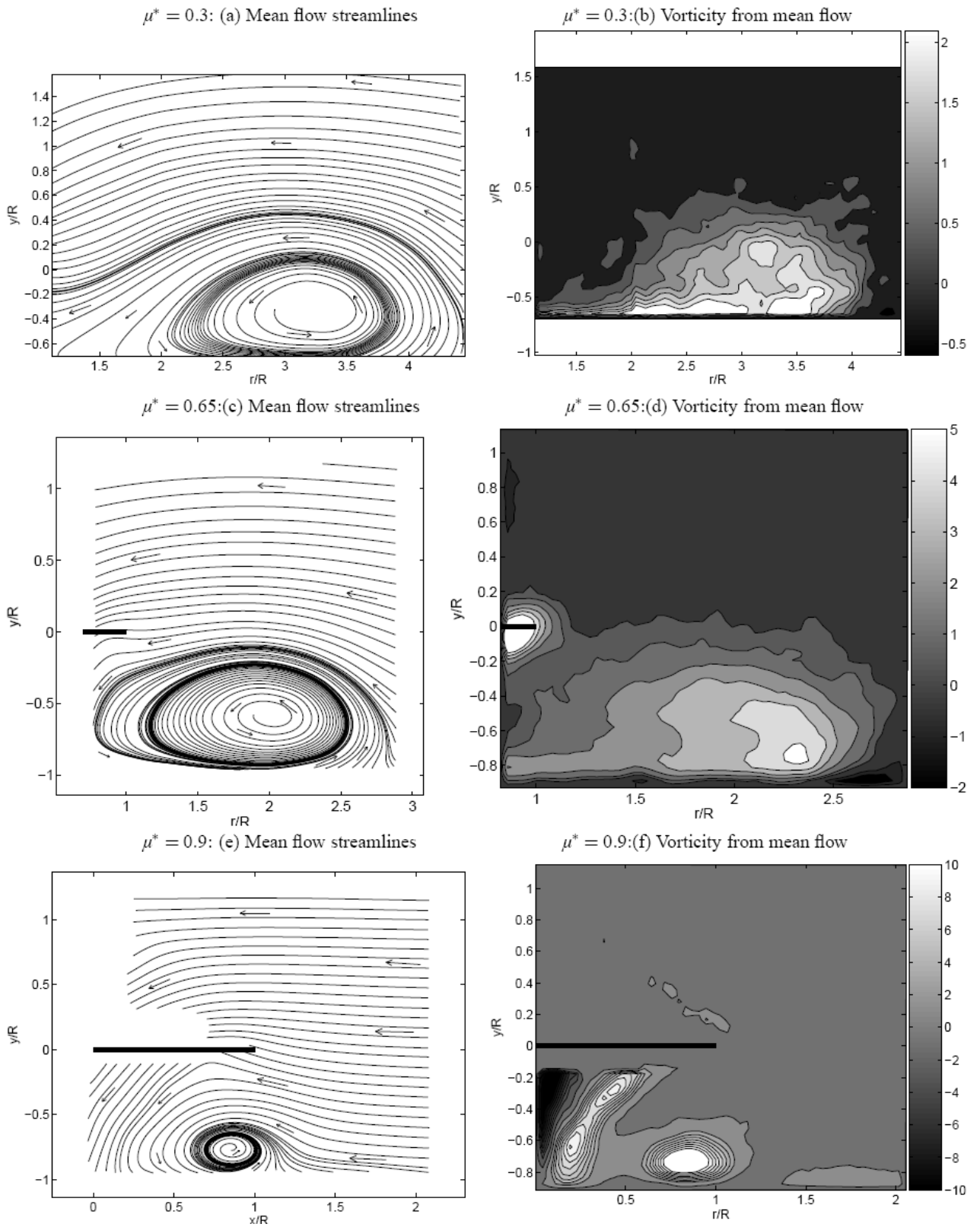

Figure 4. Mean flow streamlines and mean non-dimensional vorticity from PIV for the rotor at 0·5D above the ground for $\mu^* = 0{\cdot}3$ (frames (a) and (b)), $\mu^* = 0{\cdot}65$ (frames (c) and (d)) and $\mu^* = 0{\cdot}9$ (frames (e) and (f)). The wind-tunnel flow is from right to left. For frames (a) and (b) the field of view is from 1D to 2·5D upstream of the rotor hub, while for the higher advance ratios the field of view is smaller and includes some of the flow below the disk. The images in frames (a) and (b) are obtained using a higher resolution camera to capture the spread of the wake at this low μ^*. The vorticity scales in each frame have been changed to account for higher magnitude vorticity as normalised advance ratio increases. The low-level vorticity contours just above the leading edge of the disk in frame(*f*) are processing artefacts due to laser glare off the blades.

https://doi.org/10.1017/S0001924000003134 Published online by Cambridge University Press

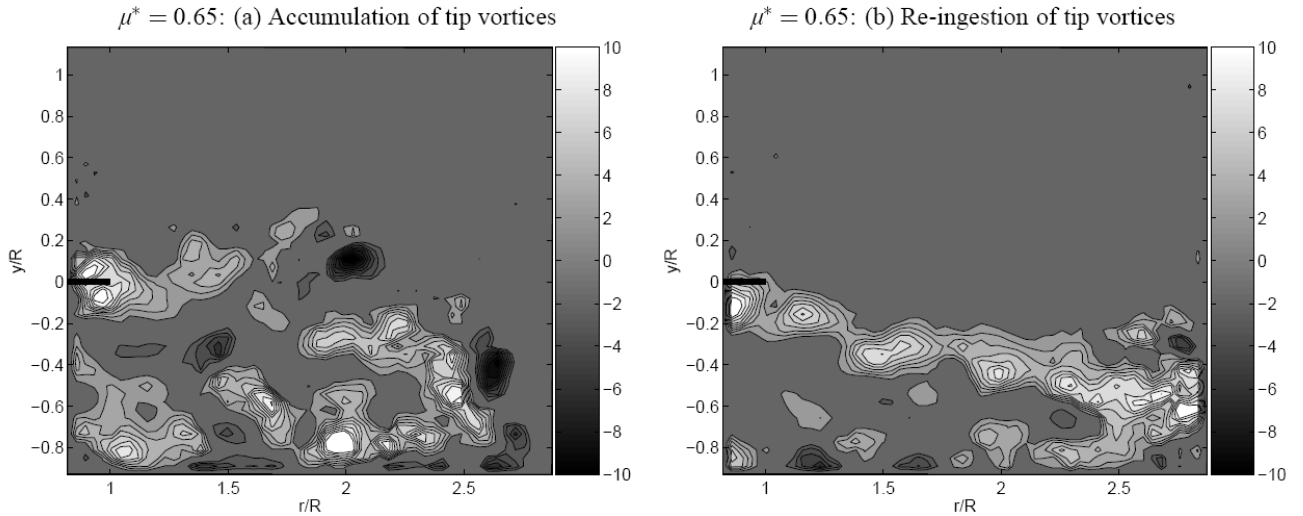

Figure 5. Instantaneous vorticity plots from PIV for the rotor at 0·5*D* above the ground for μ* = 0·65. Frame (a) shows the accumulation of the tip vortices ahead of the rotor while frame (b) shows the re-ingestion of the tip vortices through the rotor. The wind-tunnel flow is from right to left.

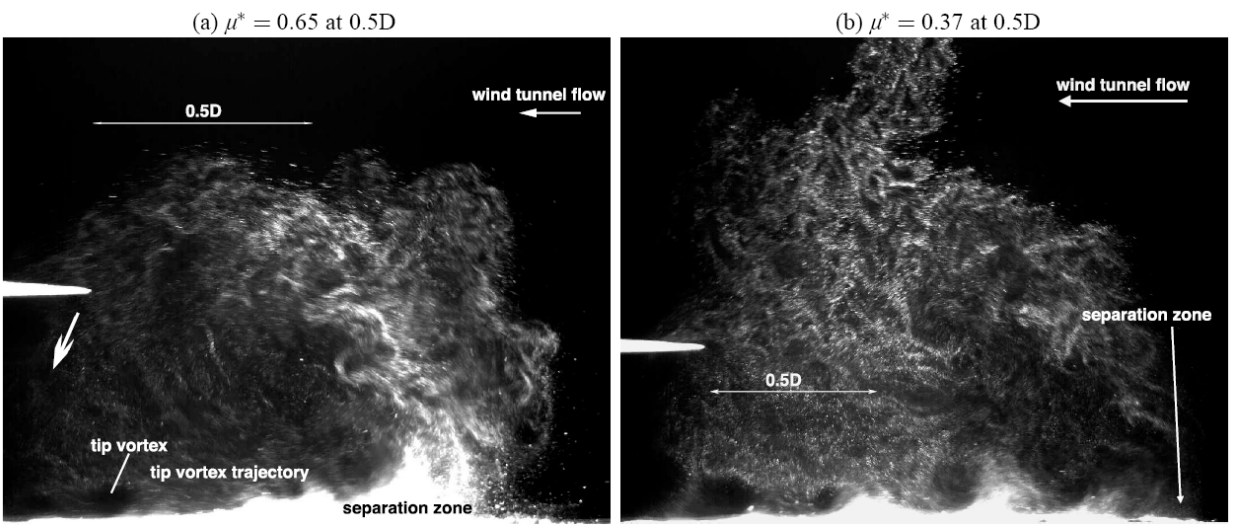

Figure 6. Still images from high speed video sequences of simulated brown-out using talcum powder spread over the tunnel floor. Rotor 0·5*D* above the ground. The leading edge of the rotor disk can be seen, and the wind-tunnel flow is from right to left. A wider field of view was required for the lower normalised advance ratio in frame (b).

mindful of the rotor start-up transient flow, video recording was completed as soon as possible after the rotor had been switched on.

A Mikrotron MotionBlitz high-speed digital video camera was used for the dust cloud visualisation experiments. This camera was capable of recording at a frame rate of 500Hz at a full-frame resolution of 1k × 1k pixels. A 5W continuous wave laser, wavelength 532nm, expanded into a thin sheet illuminated the flow ahead of the rotor, and similar regions of the flow to those for the PIV tests were viewed.

3.0 RESULTS

PIV and brown-out dust cloud flow visualisation results at relatively low normalised advance ratio will be presented in this section, as this is the condition in which the rotor is enveloped in the brown-out dust cloud. The experiments were conducted for a range of ground heights from $h/D = 0{\cdot}25$ to $h/D = 1{\cdot}0$ and normalised advance ratios of $\mu^* = 0{\cdot}3$ to $\mu^* = 1{\cdot}3$. During the experiments, the rotor was operated at a speed of 5,640RPM, with a measured out of ground effect thrust coefficient of $C_T = 0{\cdot}014$. The thrust coefficient was observed to be constant over a range of rotational speeds. The normalised advance ratio for various test cases were achieved by varying the wind-tunnel speed accordingly. A representative blade chord Reynolds number was 26,000. PIV was used to determine the (u,v) velocity field in the (r,y) plane. With the rotor in hover the PIV data indicated a tip vortex circulation Reynolds number of $\Gamma/\nu = 15{,}000$ close to the rotor disk plane. Vorticity ω is scaled with V_h/R and, where presented, velocity is scaled with V_h.

3.1 PIV investigation of the ground effect flow field

Streamlines and vorticity constructed from the mean velocity for $\mu^* = 0{\cdot}3$, $\mu^* = 0{\cdot}65$ and $\mu^* = 0{\cdot}9$ with the rotor at a height of half a diameter above the ground are shown in Fig. 4. Mean flow streamlines are useful to show in that they indicate where the brown-out dust cloud would be expected to appear. Streamline seed points are placed at selected locations in the velocity field, and the streamlines are then formed by tracing a particle released from each seed point. These flow patterns are only cartoons; the flow is three-dimensional

https://doi.org/10.1017/S0001924000003134 Published online by Cambridge University Press

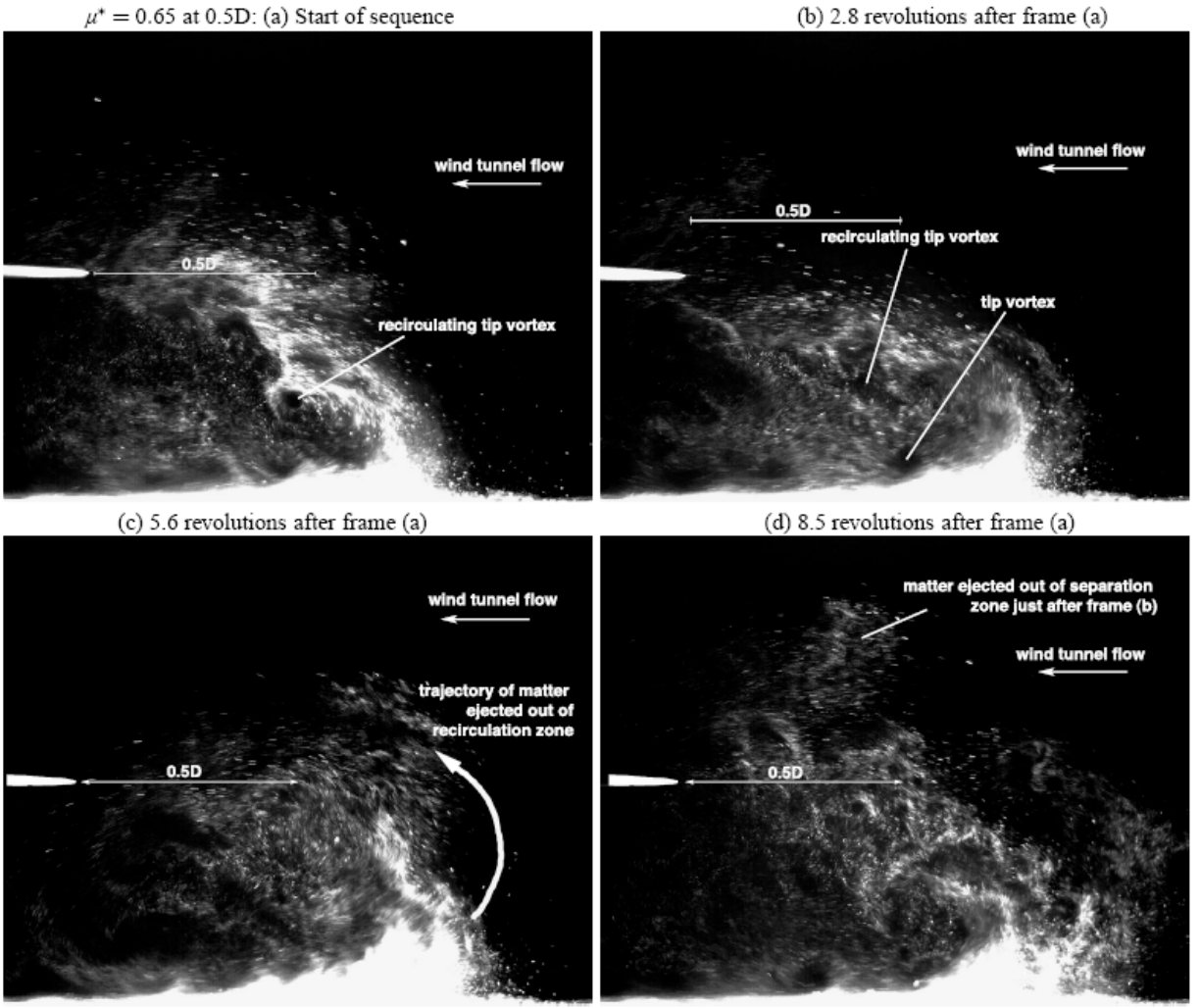

Figure 7. Still images from high speed video sequences of simulated dust cloud using talcum powder spread over the tunnel floor for the rotor 0·5*D* above the ground, μ* = 0·65. The leading edge of the rotor disk can be seen, and the wind-tunnel flow is from right to left.

and unsteady, so no streamline pattern like those in the figure would ever be observed, but they are a useful aid in interpreting the results. In the figure the rotor tip is at the co-ordinate (r/R, y/R) = (1,0), and the ground is along y/R = –1. For the lowest advance ratio the mean flow streamlines in Fig. 4 frame (a) show a gross recirculation centred around a point at just over one diameter ahead of the leading edge of the rotor disk. There is a mean flow separation point on the ground just off the far right hand side of the image, and the streamline crowding close to the ground below the recirculation zone indicates the very high fluid velocities there. Figure 4(b) shows a region of positive vorticity ahead of the rotor extending to a distance of around 4R ahead of the disk and to a height of y/R = 0·6 above the rotor disk. The thin ribbon of vorticity close to the ground at the left hand side of the image is where tip vortices track along the ground from left to right, and these tip vortices feed the recirculation zone. There is significant mean flow vorticity as high as 0·5R above the disk. As μ* increases the wake is pushed towards the rotor disk. At μ* = 0·65 the mean flow streamlines on frame (c) show the gross recirculation zone much closer to the disk, and the mean flow separation is now seen on the extreme right hand side of the image. The mean flow vorticity, frame (d), is in a smaller zone than at lower advance ratio and extends to the lower height of around y/R = 0·2 above the rotor disk, but the vorticity magnitude is higher. At high enough advance ratio the recirculation is tucked under the disk, as shown in frames (e) and (f) for μ* = 0·9. The mean flow streamlines show a very tightly packed, small bundle and mean flow separation at around r/R = 1·1. The vorticity plot on frame (*f*) shows a number of features. The mean recirculation close to the ground is clear and contains very high magnitude vorticity. The positive vorticity band reaching down and further inboard from r/R = 0·5 is the track of the blade tip vortices, and the negative vorticity band below the disk at the extreme left of the field of view is the blade root vorticity system. The effect of reducing the rotor height above the ground for a given μ* is to extend the wake further ahead of the rotor and for vorticity to extend to greater heights above the rotor disk plane.

The different regimes of the ground effect flow field identified from previous research[3,9] can be distinguished from the PIV vorticity data. At a ground distance of half a diameter, the recirculation regime was identified to exist between up to μ* = 0·6 and μ* = 0·9, while the ground vortex regime was seen to exist between μ* = 0·9 and μ* = 1·2. At the higher ground distance cases tested (up to 1 diameter in these experiments), these μ* ranges were seen to decrease, with the ground vortex regime occuring at lower μ* values.

Individual vorticity plots at μ* = 0·65 show that the tip vortices pass along the ground ahead of the rotor, leave the ground close to the mean flow separation point and initially head back towards the rotor. They are then observed to either accumulate in the recirculation region and then merge ahead of the rotor disk, or move back toward the disk to be re-ingested through the rotor (see brown-out

https://doi.org/10.1017/S0001924000003134 Published online by Cambridge University Press

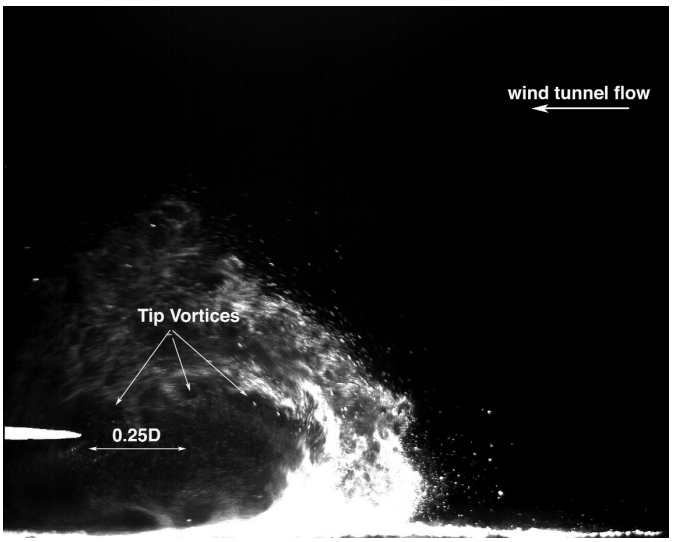

Figure 8. Still image from high speed video sequences of simulated dust cloud at $\mu^* = 0{\cdot}65$ for a ground distance of $0{\cdot}25D$. The re-ingestion of tip vortices into the rotor can be seen.

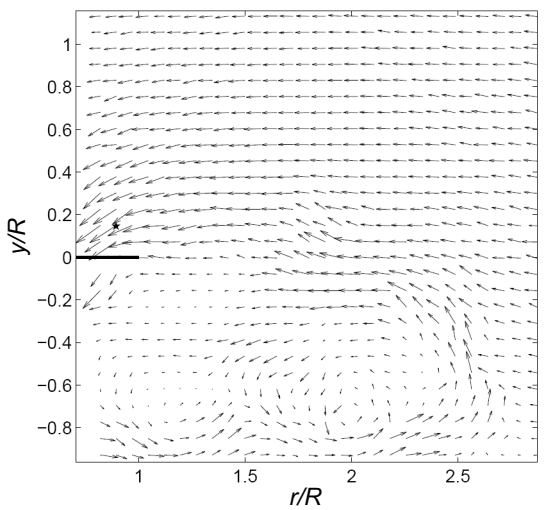

Figure 9. Instantaneous velocity field from PIV for the rotor at $0{\cdot}5D$ above the ground for $\mu^* = 0{\cdot}65$. The case shown corresponds to the vorticity plot shown in Fig. 5 frame (a). The vector with the star symbol at its root around co-ordinate (0·9,0·14) has the maximum non-dimensional velocity magnitude of 2.

investigations later). The accumulation of tip vortices at $\mu^* = 0{\cdot}65$ for a rotor height of half a diameter is shown in Fig. 5(a). This accumulation is seen to occur around the region identified in Fig. 4(d) as the location of the region of strong, mean, positive vorticity. An example of the re-ingestion of the tip vortices through the rotor is implied in Fig 5(b), where the tip vortices track back towards the rotor disk. At this ground height and particular advance ratio the re-ingestion process is observed to be intermittent and very few images show the re-ingestion state. Many of the vorticity plots actually show a combination of the re-ingestion and accumulation processes. As the advance ratio increases, the re-ingestion process becomes more dominant, until the ground vortex regime is reached. Individual velocity fields from the PIV also show that the notional separation point on the ground moves from left to right around the mean position. Regions of negative vorticity, not present in the mean flow vorticity, are also observed in the individual vorticity plots; in Fig. 5(a) two prominent clumps of strong, negative vorticity are seen at $(2{\cdot}5R, -0{\cdot}4R)$ and $(2R, -0{\cdot}2R)$, and in frames (a) and (b) zones of negative vorticity are seen close to the ground. These are not fragments of negative vorticity trailed from the rotor root, but instead they are observed to arise from the tip vortices as they travel forwards along the ground towards the mean flow separation zone, and it appears that these trailing vortices induce secondary separated flow ahead of them. Note that the PIV data presented by Ganesh *et al*[15] do not show this negative vorticity, and this warrants further investigation.

3.2 Helicopter brown-out simulation results

Figure 6 shows typical still images from the video sequences for $\mu^* = 0{\cdot}65$ and $\mu^* = 0{\cdot}37$, with the rotor positioned half a diameter above the ground. A large cloud of dust was seen to form ahead of the rotor disk leading edge. These dust clouds show the tip vortex trajectories and the separation zones on the tunnel floor also observed in the PIV. The separation zone on Fig. 6(a) is shown by the bright, white region on the right side of the image. Figure 6(b) also shows the separation point, much less clearly, further to the right than for the higher advance ratio, but the powder is observed to rise far higher above the rotor, and the contamination of the air by the action of the rotor lifting the powder off the ground is greater in coverage. The apparent wavy effect at the ground in each of these images is the powder picked up by the vortices as they pass over the ground from left to right; it is observed that the dust is picked up off the ground most vigorously just to the lower right of the tip vortices.

A series of snapshots shown in Fig. 7 for a ground distance of half a diameter and $\mu^* = 0{\cdot}65$ traces the path of the trailed vortices along the ground and higher into the wake. Figure 7(a) indicates a trailing vortex that has travelled to the right along the ground from below the rotor disk, left the ground at the separation point, moved up into the dust cloud and then started to approach the rotor blade. There are trailing vortices close to the ground below and to the left of the tip vortex indicated. Note that the dust cloud seen is the accumulated effect of a few thousand rotor revolutions of flow. Close to the ground the dust particle velocity is high, and dust particle images appear as blurred streaks due to the camera exposure time. Large clumps of powder are picked up by the tip vortices close to the ground as they approach the separation zone. While much of the material appears to follow the air flow to form the dust cloud, some of the dust passes through the separation zone, revealed by the large, white particles in the flow to the right of the separation zone; the lighter of these particles are forced back towards the separation zone by the wind-tunnel flow, while the heavier ones land on the ground to the right. As the indicated trailing vortex in frame (a) moves back towards the rotor, it is seen to accelerate the tip vortices closer to the ground below which are already moving to the right, frame (b). This appears to enhance the rate of dust pick up off the ground, and these features are shown in Fig. 7(b), (c) and (d). Associated with the rapid movement to the right of the tip vortex indicated in frame (b), there is a particularly energetic expulsion of matter out of the separation zone just after frame (b); the fate of this dust is indicated in frames (c) and (d) and its height above the rotor disk is noteworthy. Note that the PIV could not provide a time-resolved flow history. Figure 8, for $\mu^* = 0{\cdot}65$ at a ground height of $0{\cdot}25D$, shows tip vortex reingestion, but also shows the dust cloud extending high above the rotor disk to a height similar for the same normalised advance ratio with the rotor at a greater height above the ground. Another major observation from the brown-out videos is the three dimensionality of the flow. Clouds of powder, originating from elsewhere in the flow can appear in the plane of view of the flow being monitored. Similarly, dust originating within the plane of view can be seen disappearing from view. This has been attributed to the strong cross-flow components present within the ground effect flow field.

https://doi.org/10.1017/S0001924000003134 Published online by Cambridge University Press

4.0 DISCUSSION

Quantitative and qualitative data from experimental measurements of the flow around a rotor in ground effect in low speed forward flight have been presented. The rotor in these experiments was not trimmed in any way, and the ground was also stationary relative to the rotor hub. Trim could be achieved in a real helicopter by centre of gravity position and use of cyclic pitch. In this experiment c.g. position is irrelevant, so it may be argued that the trim state of the isolated rotor is of little significance, but for the purposes of comparison of these tests with other experiments on isolated rotors it does become meaningful. Relative velocity effects at the ground are without doubt important for the wake development, but the basic fact remains that the ground effect wake is the result of the rotor trailing vortices spreading over the ground. Thus, while the current experiments in no way are designed to generate performance data, they provide a useful platform for qualitative (and limited quantitative) analysis of the ground effect flow. PIV was used to measure the velocity in selected areas around the rotor, and the magnification used allowed the image processing algorithms to produce high fidelity velocity maps. Velocity histograms are used in PIV to reveal systematic bias errors[18], and the only velocity clustering observed from the PIV results tended to occur around the imposed wind-tunnel speed and around zero velocity (corresponding to masked out-of-bounds areas and low magnitude u and v components). This lack of clustering around other values of velocity indicates a well conditioned experiment and analysis for PIV, notwithstanding loss of detail associated with the low spatial resolution of the PIV in the vortex cores. Dust cloud flow visualisation experiments to simulate brown-out have proven to be highly effective, and the dust pick-up by the rotor flow and the subsequent evolution of the dust cloud can be seen.

A comparison of the PIV results with some previous ground effect research is presented in table 1. Similar values for the various ground effect flow regimes were obtained for comparable rotor ground distances in research done by Ganesh *et al*[12]. Their experiments were conducted at larger scale in a wind tunnel but is not clear what thrust coefficients their experiments were operating at. Comparisons with Curtiss *et al*[3] showed greater differences in terms of the μ^* values at which different GE flow regimes were observed to occur, however. This difference is observed because of the inherent differences in the experimental conditions between the two sets of tests; Curtiss *et al* used a towing facility, with a helicopter model moving over ground, while the PIV tests were conducted in a wind tunnel with a stationary ground. The ground boundary condition is quite different, and in the wind tunnel there is the additional problem caused by formation of a ground boundary layer on the ground plane. Assuming that the ground board is a flat plate, the average boundary-layer thickness at the various locations the rotor was placed on the ground board was calculated to be around 1cm; when scaled with respect to the rotor radius, this amounts to 0·15R. Both the PIV and brown-out flow visualisation tests suggested secondary flow separation at the ground caused by the passage of the trailing vortices, and the presence of the ground boundary layer ahead of the rotor must be affecting this process. This issue should be addressed in conjunction with modelling the moving ground boundary condition.

Table 1
Comparison of ground effect flow regimes with other investigators

	Curtiss *et al*[3]	current data
Rotor height	**0·45*D***	**0·5*D***
Regime:		
Recirculation	$0{\cdot}4 < \mu^* < 0{\cdot}64$	$0{\cdot}6 < \mu^* < 0{\cdot}9$
Ground Vortex	$0{\cdot}64 < \mu^* < 0{\cdot}83$	$0{\cdot}9 < \mu^* < 1{\cdot}1$
	Ganesh *et al*[12]	current data
Rotor height	**0·36*D***	**0·5*D***
Regime:		
Recirculation	$0{\cdot}03 < \mu < 0{\cdot}05$	$0{\cdot}044 < \mu < 0{\cdot}07$
Ground Vortex	$0{\cdot}06 < \mu < 0{\cdot}08$	$0{\cdot}08 < \mu < 0{\cdot}09$

At the lowest forward flight speed tested ($\mu^* = 0{\cdot}3$) the PIV results show the presence of mean flow separation and a region of mean, positive vorticity (anti-clockwise) ahead of the rotor, which was seen to increase in strength, reduce in size, and to form nearer the rotor leading edge as μ^* increased. Although the general flow features at $\mu^* = 0{\cdot}3$ and $\mu^* = 0{\cdot}65$ are similar, the two cases are considered to represent different regimes of the ground effect flow field. This distinction within the flow field was made by considering the path taken by the trailing vortices around the region of mean, positive vorticity. Only when the trailing vortices are re-ingested through the rotor was the flow considered to be in the recirculation regime[3,12]. For the current test conditions at least, a comparison of the PIV results and

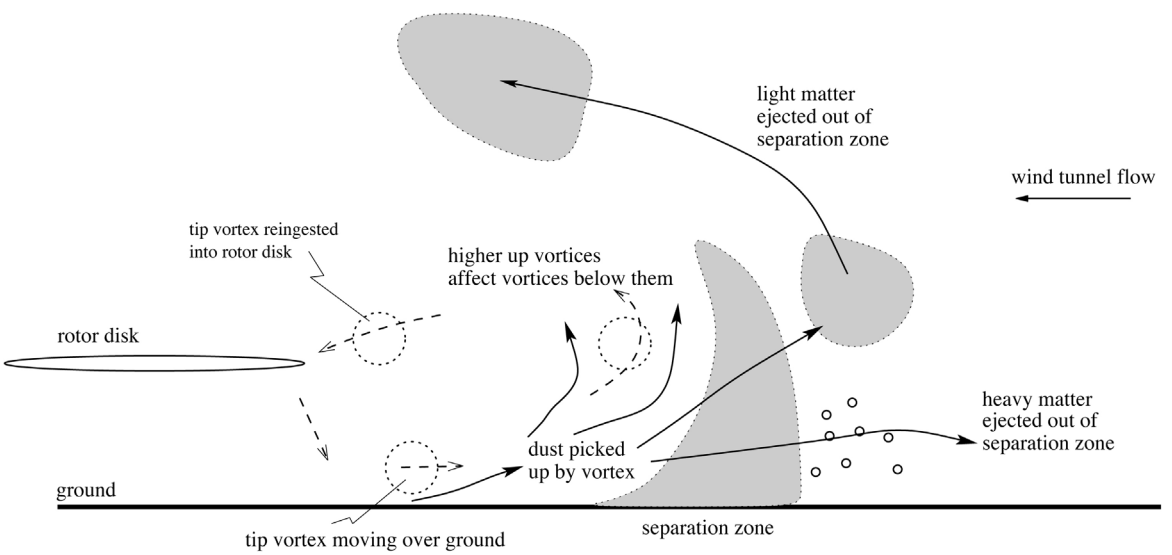

Figure 10. Schematic diagram of the dust cloud simulation in Fig. 7. Vortex and dust particle trajectories are indicated by the dashed and solid lines respectively, and selected areas of dust particle laden flow are highlighted.

https://doi.org/10.1017/S0001924000003134 Published online by Cambridge University Press

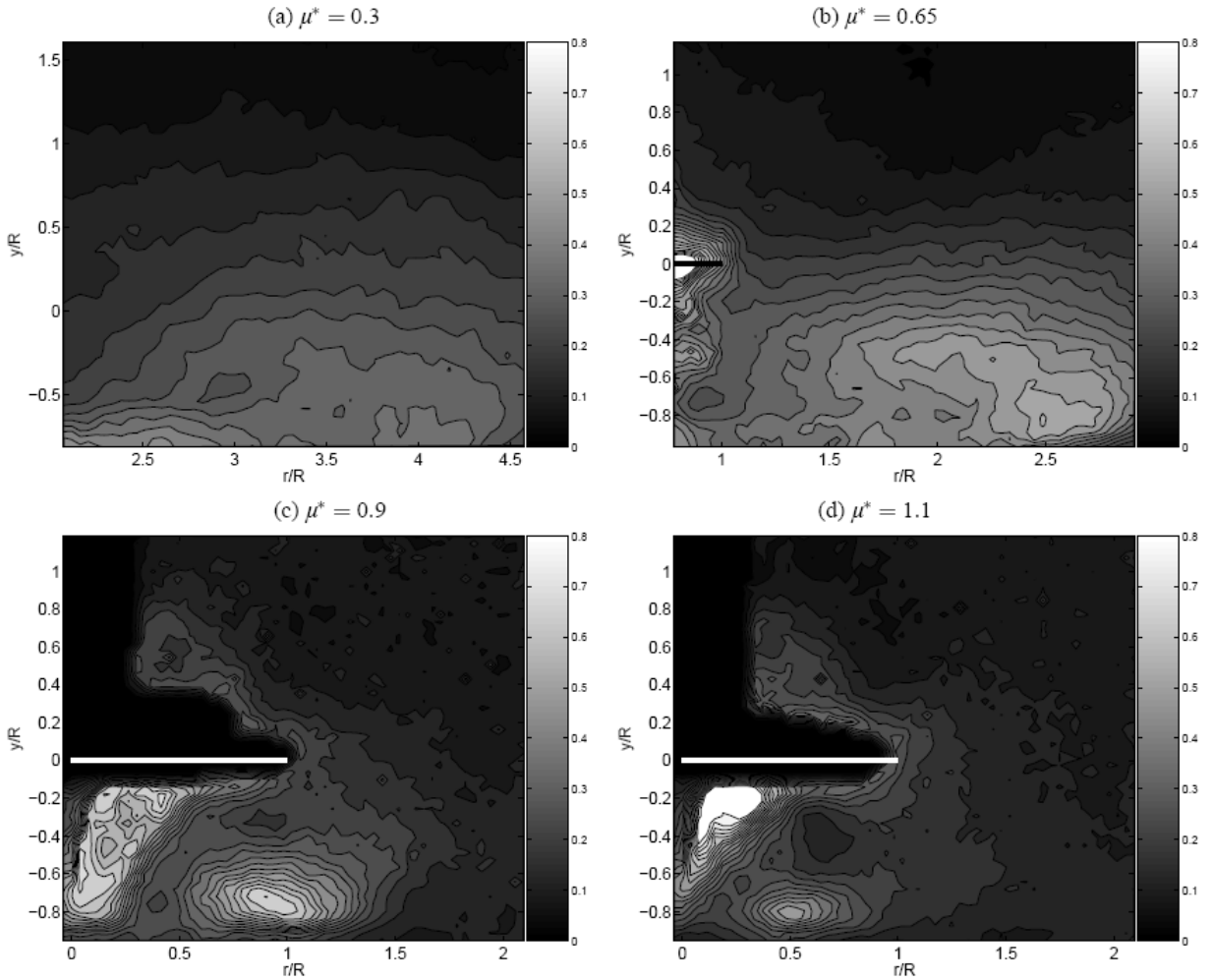

Figure 11. Root mean square of velocity fluctuations around the mean from PIV for the rotor at 0·5D above the ground for $\mu^* = 0{\cdot}3$, $\mu^* = 0{\cdot}65$, $\mu^* = 0{\cdot}9$ and $\mu^* = 1{\cdot}1$. Note the much larger area of flow imaged in frame (a) at $\mu^* = 0{\cdot}3$. The large, black areas in frames (c) and (d) above the disk and inboard of the tip are masked areas indicating the presence of the blade and rotor apparatus. The wind-tunnel flow is from right to left.

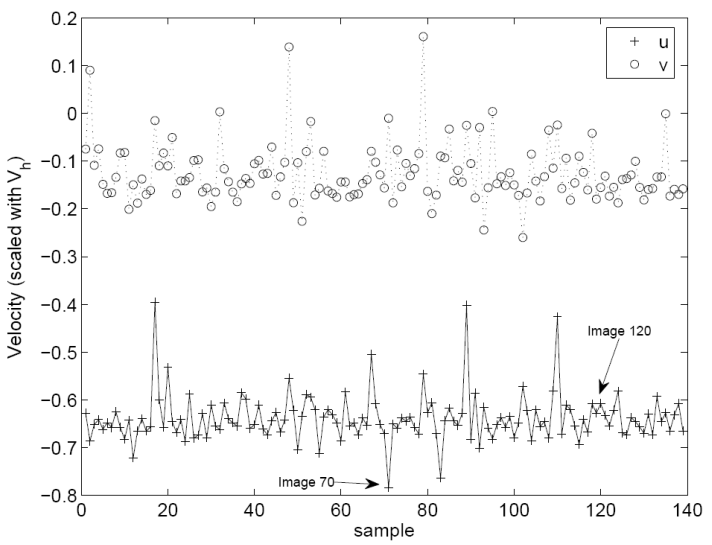

Figure 12. Velocity fluctuations at (*r/R, y/R*) = (2·0, 0·8). The rotor is 0·5*D* above the ground and $\mu^* = 0{\cdot}35$.

https://doi.org/10.1017/S0001924000003134 Published online by Cambridge University Press

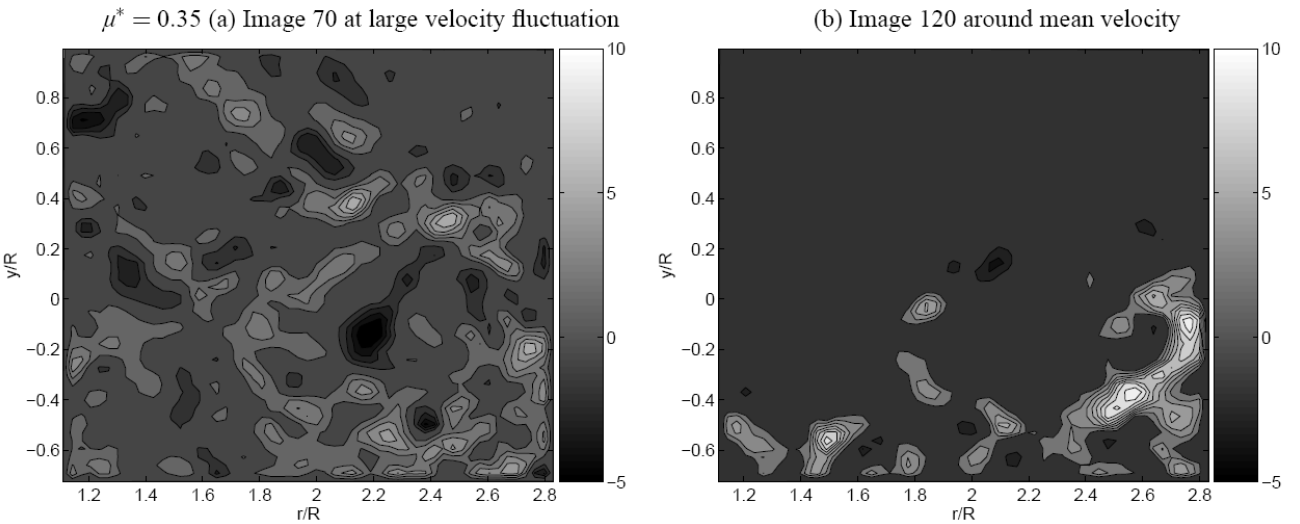

Figure 13. Individual vorticity plots for the two cases indicated on Fig. 12. Rotor at ground height of 0·5*D* and μ* = 0·35. Frame (a) shows a plot where the vorticity reaches high above the rotor, while frame (b) shows little vorticity above the plane of the disk. The wind-tunnel flow is from right to left.

the dust cloud tests shows that the main dust cloud extends at least as far forward as the mean vorticity below the rotor. This can be seen when comparing Figs 4 and 6. In Fig. 4(d) the positive vorticity region extends as far forward as about r/R = 2·6, while in Fig. 6(a) for the same μ* = 0·65, the cloud extends forward by just under 2*R* forward of the tip of the disk, equivalent to just under 3*R* from the hub. The equivalent values for μ* = 0·65 are just over 4*R* for the PIV vorticity (as shown in Fig. 4(b)) and 3·8*R* for the dust cloud (as shown in Fig. 6(b)), although the flow visualisation test was conducted at the higher value of μ* = 0·37 where the dust cloud would be smaller. Inspection of the flow visualisation movie sequences shows that while dust patterns close to the ground show rotation corresponding to positive vorticity, those parts of the dust cloud high up above the ground show no preferred sense of rotation. Meanwhile the PIV shows only weak positive or negative vorticity extending far above the level of the rotor disk, but where the dust cloud extends the highest above the ground the vorticity (or at least the lateral component resolvable in these experiments) is of low magnitude and no preferred sign.

It is well known that the processes of surface traction, saltation and suspension are responsible for wind-induced movement of loose material on the ground[19]. These affect the surface material as follows: in the case of surface traction the material is dragged over the ground but never becomes airborne; in the saltation process material becomes airborne but it eventually returns to the surface; and in the case of suspension the material remains airborne and does not return to the ground. In general the surface shear τ is important to consider, and there is a critical shear stress that initiates saltation. The PIV and the dust cloud visualisation show the tip vortices to track rapidly across the ground. PIV shows very high velocities just above the ground in the vicinity of the tip vortices, which implies high shear. Figure 9 shows the velocity field corresponding to the vorticity case presented in Fig. 5(a) for μ* = 0·65. Here distinct zones of high magnitude velocity are seen close to the ground, and these are around the locations of the tip vortices. Close examination of the flow visualisation shows dust particles becoming airborne just ahead of the tip vortices as they approach from the left, and this would appear to be broadly coincident with the high velocity magnitude zones seen close to the ground in the PIV. These measurements suggest high shear in these zones. Also the direction of flow just above the surface where the velocity magnitude is high tends to be away from the ground, which would then sweep the dust to the right and upwards. While the vortex cores are inevitably devoid of heavy material, the very close proximity of the tip vortices to the ground as they pass over the ground mean that vorticity bearing fluid is tagged with the ground dust. Vortex lines move with the fluid, while dust follows its own trajectory dependent upon the size and relative density of the dust particle. Smaller dust particles will tend to follow the flow relatively closely, and for this reason the recirculation zone ahead of the rotor disk becomes heavily contaminated by the dust. Larger dust particles will be ejected from regions of high spatial and temporal acceleration to contaminate the wider flow field. Figure 10 shows a schematic diagram of the sequence leading to the formation of the dust cloud.

A more sensitive indicator from the PIV data of the likely presence of ground dust in the flow field might be the velocity fluctuation. Velocity fluctuation statistics are conveniently represented by the root-mean-square (RMS) of the velocity fluctuations about the mean from the PIV data. Figure 11 shows the RMS velocity distribution of the ground effect wake at different forward flight speeds with a rotor height of half a diameter above the ground. The reader should note the much larger area of flow imaged in frame (a) at μ* = 0·3. The lower μ* cases, frames (a) and (b) possess lower velocity fluctuations compared with the ground vortex flow regimes at higher μ* in frames (c) and (d), but the velocity fluctuations are seen to affect a greater proportion of the flow field. The greatest magnitudes of the unsteadiness are observed closer to the ground, and the velocity fluctuations are seen to be of very low magnitudes above the rotor disk. In the ground vortex regimes, the velocity fluctuations are seen to be concentrated around the location of the ground vortex itself. The surrounding flow field is observed to possess very low velocity fluctuations, implying the ground vortex regime to be the steadier regime when compared with the recirculation flow regime. Dust cloud observations at μ* = 0·37 showed the flow high above the disk to show occasional bursts of dust, but this intermittent behaviour is not reflected in the RMS velocity plots. Examining the PIV velocity history at specific points in the flow, much like placing a hot-wire probe at a particular location, reveals an interesting behaviour (note the PIV is not time-resolved, so the periodicity of the velocity fluctuations cannot be determined). An example of this is shown in Fig. 12, which shows the *u* and *v* velocity component fluctuations at the point (r/R, y/R) = (2·0, 0·8) in the flow field for the rotor at a ground height of half a diameter and μ* = 0·35. The figure shows occasional bursts of much higher or lower velocity relative to the mean. Individual vorticity plots, corresponding to a mean velocity case and a large velocity deviation case

https://doi.org/10.1017/S0001924000003134 Published online by Cambridge University Press

indicated on Fig. 12, are shown in Fig. 13. The difference between the two frames is clear and around $(r/R, y/R) = (2{\cdot}0, 0{\cdot}8)$ frame (a) shows the presence of moderate vorticity concentrations, while frame (b) shows no significant vorticity in the area. This corresponds well to the observations of occasional large dust clouds made during the flow visualisation tests, although some further investigation is necessary.

5.0 CONCLUSION

An investigation of ground effect has been performed. The experiments conducted allowed for both qualitative and quantitative analysis of large areas of the ground effect flow field. Two-component velocity measurements and the vorticity field and RMS velocity fluctuations helped characterise the ground effect flow. Comparisons of the PIV data with previous research were good even though the experiments were conducted in a wind tunnel with a stationary ground. From the PIV tests, it was established that the recirculation regime consisted of a region of vorticity spread over a relatively large distance of the flow along the ground. Re-ingestion of tip vortices was occasionally observed at the lower advance ratios of the recirculation regime, and this became more common with increasing advance ratio and decreasing rotor heights above the ground. Of particular significance at lower advance ratio is the track of individual tip vortices over the ground ahead of the rotor.

The brown-out phenomenon simulated in the wind tunnel showed the influence of the tip vortices on the dust cloud ahead of the rotor. At the normalised advance ratios tested, the tip vortices were either seen to accumulate ahead of the rotor disk, resulting in more powder being picked up and building up the dust clouds to reach greater heights, or were observed to be re-ingested through the rotor disk. Dust pick-up was especially vigorous in the immediate vicinity of the tip vortices passing over the ground. Comparisons of the dust cloud and PIV tests show the dust cloud broadly coincident with the regions of mean flow recirculation and high vorticity identified from the PIV plots, although the dust cloud was seen to reach greater heights than the region of strong, mean vorticity. Occasional bursts of dust were observed at these heights, which may be associated with large velocity fluctuations from the local mean observed in the PIV. The results presented in this paper have been obtained from tests which are not true experimental simulations of a rotor operating near the ground. Firstly the ground is stationary relative to the wind, and the ground plane has a boundary layer over it. While the boundary layer may not affect the gross features of the flow field which were investigated in this paper, more sophisticated experiments with a moving ground and more advanced rotor rigs are necessary if a complete investigation of the rotor in ground effect is to be conducted.

ACKNOWLEDGEMENTS

This work was conducted with the financial support of the United Kingdom Ministry of Defence and Qinetiq plc under PO number CDAIR-04619. The contributions of the technical staff at the Acre Road wind-tunnel facility at the University of Glasgow are appreciated. Insightful guidance was provided by Professor R. Brown, Dr W. Chan and Mr I. Simons.

REFERENCES

1. ZBROZEK. J. Ground effect on the lifting rotor, British ARC, R & M No 2347, July 1947.
2. FRADENBURGH, E.A. The helicopter and the groundeffect machine. *J American Helicopter Society*, October 1960, **5**, (4), p 24.
3. CURTISS, H.C., SUN, M., PUTMAN, W.F. and HANKER, E.J. Rotor aerodynamics in ground effect atlow advance ratios, *J American Helicopter Society*, 1984, **29**, (1), pp 48–55.
4. LEISHMAN, J.G. *Principles of Helicopter Aerodynamics*, 2nd Ed Cambridge Aerospace Series. Cambridge University Press, Cambridge, UK, 2006.
5. CURTISS, H.C., ERDMAN, W. and SUN, M. Ground effect aerodynamics, *Vertica*, 1987, **11**, (1-2), pp 29–42.
6. HAYDEN, J.S. The effect of the ground on helicopter hovering power required. 32nd Annual Forum of the American Helicopter Society, May 1976.
7. BROWN, R.E. and WHITEHOUSE, G.R. Modelling rotorwakes in ground effect, *J American Helicopter Society*, 2004, **49**, (3), pp 238–249.
8. SHERIDAN, P.F. and WIESNER, W. Aerodynamics of helicopter flight near the ground. In 33rd Annual Forum of the American Helicopter Society, May 1977.
9. GANESH, B.A. and KOMERATH, N. Unsteady aerodynamics of rotorcraft in ground effect. In 22nd Applied Aerodynamics Conference and Exhibit, Providence, Rhode Island, USA, 16-19 August 2004.
10. SAIJO, T., GANESH, B., HUANG, A. and KOMERATH, N. Development of unsteadiness in a rotor wake in ground effect, In 21st AIAA Applied Aerodynamics Conference, Orlando, Florida, USA, June 2003.
11. PULLA, D. and CONLISK, A. The long term structure of a rotor wake in ground effect. In 43rd AIAA Aerospace Sciences Meeting and Exhibit, Reno, Nevada, USA, January 2005.
12. GANESH, B.A., KOMERATH, N., PULLA, D. and CONLISK, A. Unsteady aerodynamics of rotorcraft in ground effect. In 43rd Aerospace Sciences Meeting and Exhibit, Reno, Nevada, USA, January 2005.
13. BOYD, E.A. and KUSMARWANTO, I. Ground effect on a rotor wake. In Cranfield Institue of Technology, College of Aeronautics, Cranfield, UK, Report 8323, 1983.
14. KUSMARWANTO, I. Ground Effect on a Rotor Wake, PhD thesis, Cranfield Institute of Technology, College of Aeronautics, Cranfield, UK, March 1985.
15. GANESH, B.A. and KOMERATH, N. Study of groundvortex structure of rotorcraft in ground effect atlow advance ratios. In 24th Applied Aerodynamics Conference, San Francisco, California, USA, 5-8 June 2006.
16. CHEN, A.L., JACOB J.D. and SAVAS, Ö. Dynamics of corotating vortex pairs in the wakes of flapped airfoils, *J Mechanics*, 1999, (382), pp 155–193.
17. RAMASAMY, M. and LEISHMAN, J.G. Benchmarking piv with ldv for rotor wake vortex flows. In 24th AIAA Applied Applied Aerodynamics Conference,number AIAA 2006-3479, San Francisco, CA, USA, 5th-8th June 2006.
18. RAFFEL, M., WILLERT, C.E. and KOMPENHANS, J. *Particle Image Velocimetry. A Practical Guide*, 1998, Springer – Verlag Berlin Heidelberg.
19. WHITE, B.R. Soil transport by winds on Mars, *J Geophysical Research*, August 1979, **84**, pp 4643–4651.